

Theoretical investigation on Atomic Oxygen Erosion Mechanisms of 1, 3 - Didecyl Cyclopentane, 1, 3 - Dioctyldodecyl Cyclopentane and Alkylated Cyclopentane

Jingyan Nian,^a Ping Gao,^a Yongcheng Wang,^c Zhiguang Guo,^{a,b,*} Weimin Liu^a

^a State Key laboratory of Solid Lubrication, Lanzhou Institute of Chemical Physics, Chinese Academy of Sciences, Lanzhou 730000, China

^b Hubei Collaborative Innovation Centre for Advanced Organic Chemical Materials and Ministry of Education Key Laboratory for the Green Preparation and Application of Functional Materials, Hubei University, Wuhan 430062, People's Republic of China.

^c College of Chemistry and Chemical Engineering, Northwest Normal University, Lanzhou 730070, China

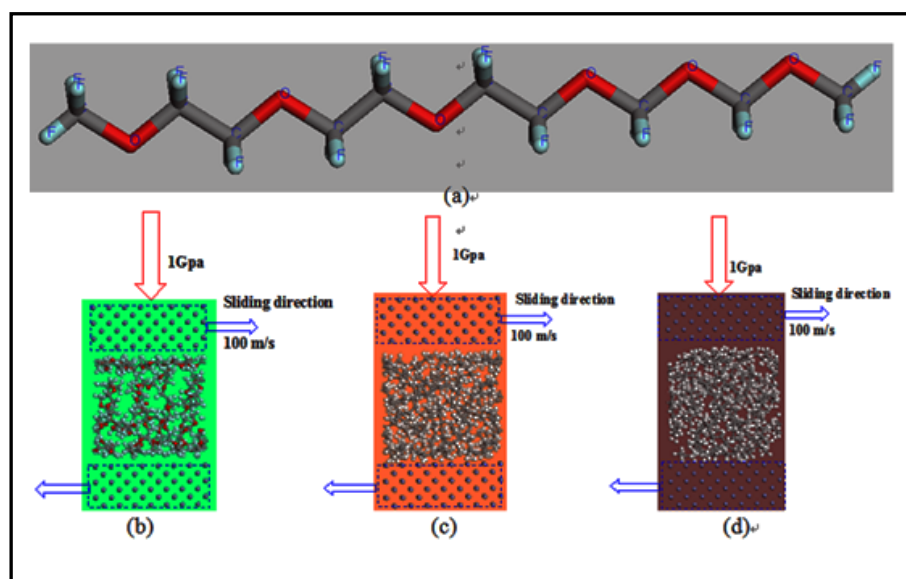
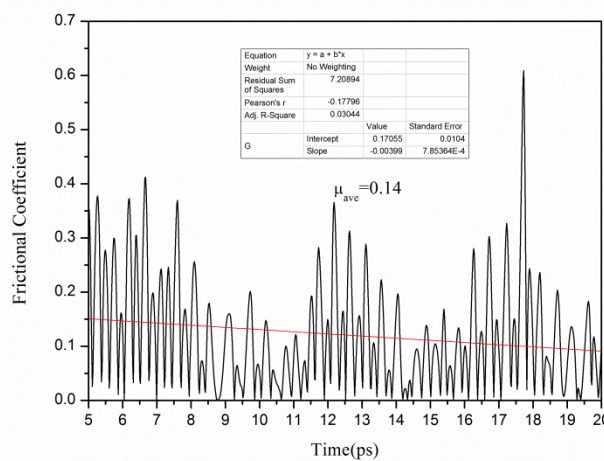
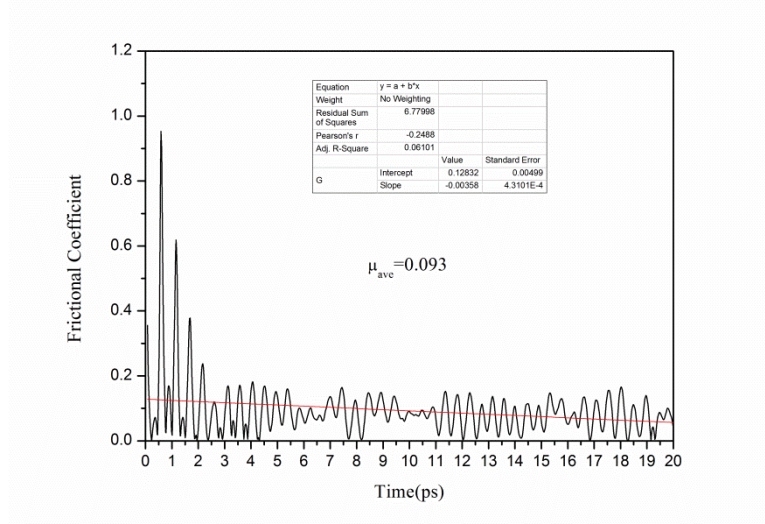


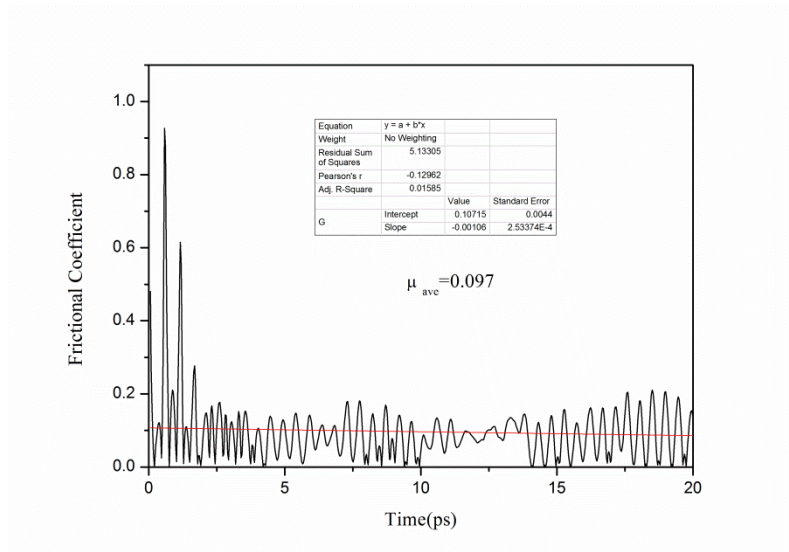
Fig 1(a): Structure of linear conjugated perfluoropolyether fragment (PFPE). **(b):** The first Confined Shear simulation model, linear conjugated perfluoropolyether as lubricants. **(c):** The second Confined Shear simulation model, 1, 3-didecyl cyclopentane as lubricant. **(d):** The third MD simulation model, and 1, 3-dioctyldodecyl cyclopentane as lubricant.



(a)



(b)



(c)

Fig 2. (a): Frictional coefficient curve corresponds to linear conjugated perfluoropolyether. **(b):** Friction coefficient curve corresponds 1, 3-didecyl cyclopentane. **(c):** Friction coefficient curve correspond to 1, 3-diptyldodecyl cyclopentane.

Simulation calculation results showed that: the synthesized lubricants have the lower frictional coefficients compared with the linear conjugated perfluoropolyether.

Species	Gibbs Free Energy(a.u.)	Relative free energy(eV)	Imaginary frequencies(in cm⁻¹)
³ IM 1	-389.4012	0.00	
³ TS 1	-389.3158	2.32	757.38 i
³ IM 2	-389.4281	-0.73	
³ IM3	-389.4317	-0.83	
³ TS 2	-389.2619	3.79	843.71 i
³ IM4	-389.3251	2.07	
C ₃ H ₇ O•	-271.0158	0.00	
² TS 3	-270.9810	0.95	237.72 i
² IM 5	-270.9984	0.47	
² IM 6	-154.3383	0.00	
² TS 4	-154.2995	1.05	
² IM 7	-154.3110	0.74	790.41 i
³ IM8	-153.6928	0.00	
³ TS 5	-153.6583	0.94	858.10 i
³ IM 9	-153.6720	0.57	
² IM 10	-153.1665	0.00	
² TS 6	-153.1417	0.67	236.65 i
² IM 11	-153.1504	0.44	
C ₅ H ₉ O•	-271.015807	0.00	
² TS 7	-270.9810	0.95	951.85 i
² IM 12	-270.9984	0.47	
³ IM 13	-345.7171	0.00	
³ TS 8	-345.5637	4.17	662.12 i
³ IM 14	-345.6871	0.82	
³ IM 15	-307.4660	0.00	
³ TS9	-307.4430	0.63	262.10 i
³ IM 16	-307.4602	0.16	
³ IM 17	-189.5880	0.00	
³ TS 10	-189.5713	0.45	1101.83 i
³ IM 18	-189.5918	-0.10	
² IM 19	-189.0875	0.00	
² TS 11	-189.0786	0.24	985.52 i
³ IM 20	-189.0969	-0.26	
³ IM 21	-507.2626	0.00	
³ TS 12	-507.1787	2.28	726.79 i
³ IM 22	-507.2963	-0.92	
¹ IM 1	-389.5426	0.00	
¹ TS 1-2	-389.4482	2.57	1848.03 i
¹ IM 2	-389.5333	-2.32	
¹ IM 5	-345.7171	0.00	
¹ TS 2	-345.5637	4.17	820.06 i
¹ IM 6	-345.6871	0.82	
¹ IM 7	-189.7446	0.00	
¹ TS 3	-189.7319	0.34	642.96 i
¹ IM 8	-189.7523	-0.21	

Table 1: Gibbs free energy, relative Gibbs free energy and imaginary frequency of all transition states calculated at level of B3LYP/ 6-311g (2d, 2p).

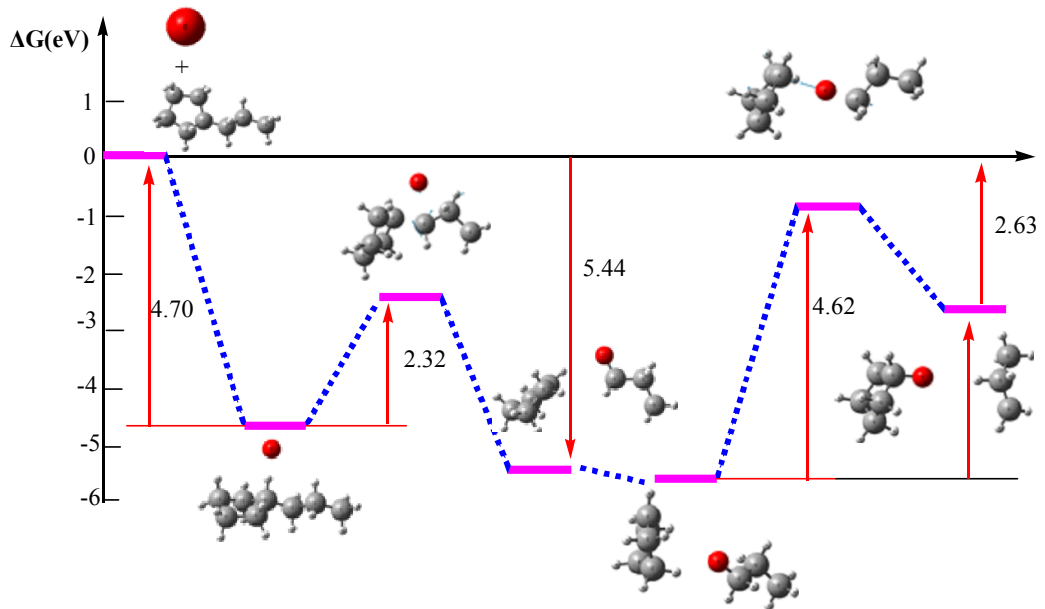


Fig 3. The triplet potential energy surface diagram corresponds to $\text{L}_1 + {}^3\text{O} \rightarrow \text{C}_5\text{H}_9\text{O}\cdot + \text{C}_3\text{H}_7\cdot$

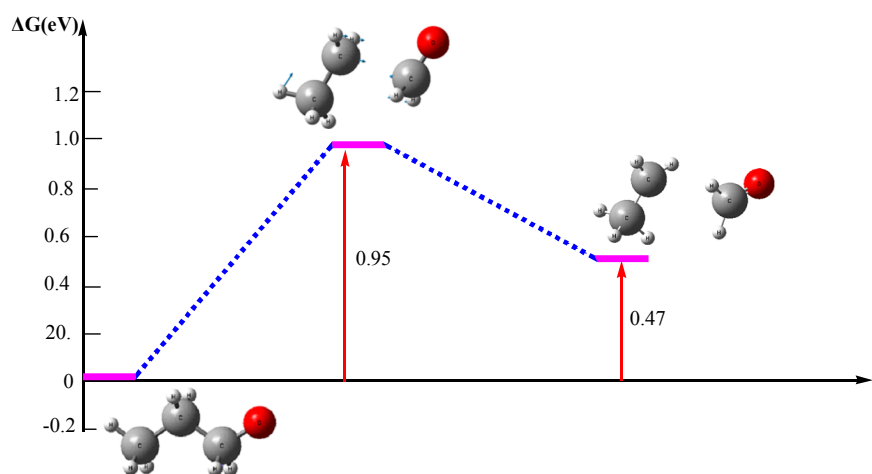


Fig 4. The doublet potential energy surface diagram corresponds to $\text{C}_3\text{H}_7\text{O}\cdot \rightarrow \text{C}_2\text{H}_5\cdot + \text{CH}_2\text{O}$.

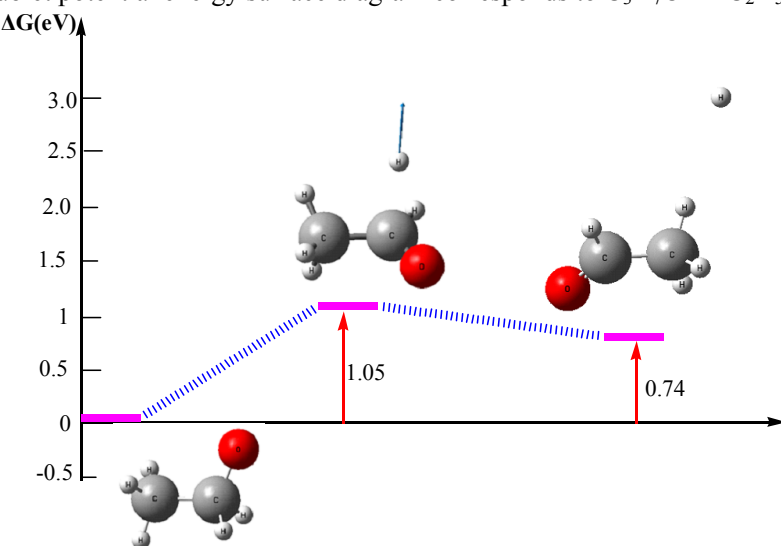


Fig 5. The doublet potential energy surface diagram corresponds to $\text{C}_2\text{H}_5\cdot + {}^3\text{O} \rightarrow \text{C}_2\text{H}_4\text{O}\cdot + \text{H}$.

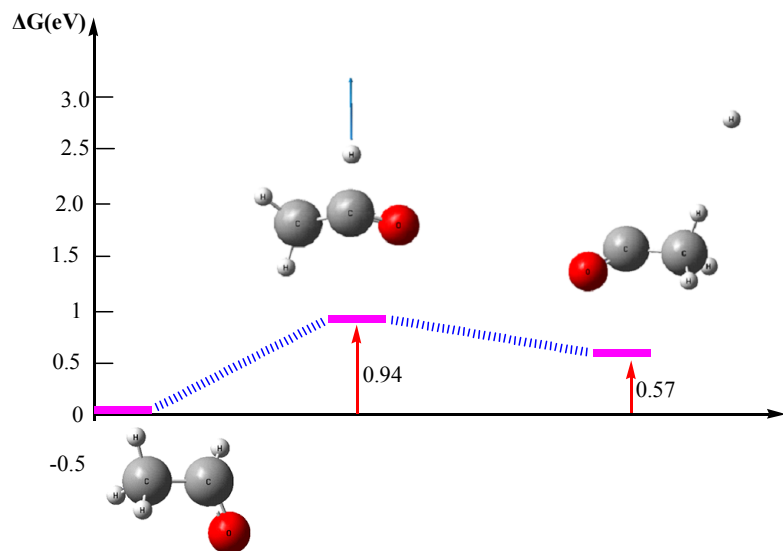


Fig 6.The triplet potential energy surface diagram corresponds to $\text{C}_2\text{H}_4\text{O}\cdot + {}^3\text{O} \rightarrow \text{C}_2\text{H}_3\text{O}\cdot + \text{H}$.

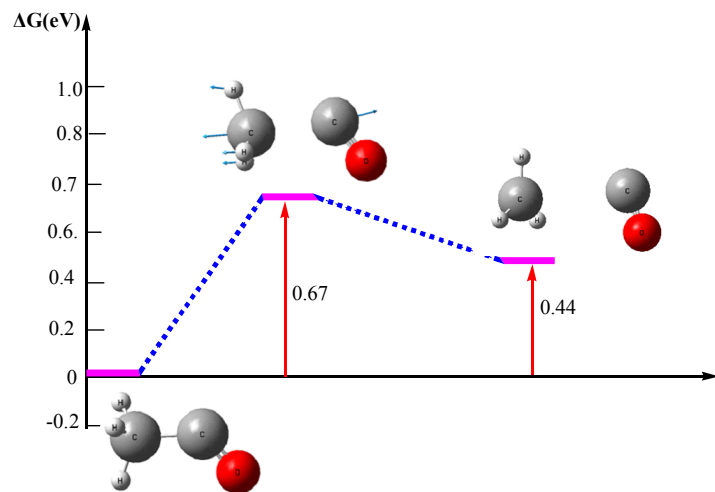


Fig 7.The triplet potential energy surface diagram corresponds to $\text{C}_2\text{H}_3\text{O}\cdot \rightarrow \text{CH}_3\cdot + \text{CO}$.

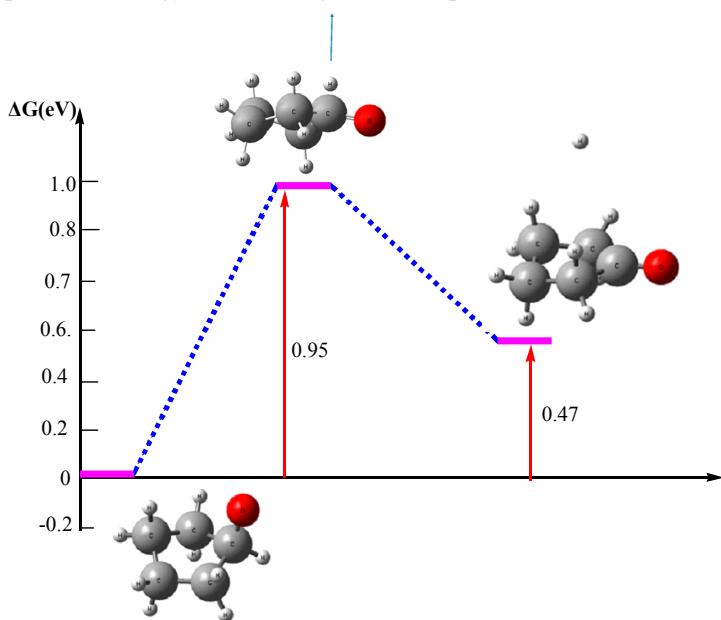


Fig 8.The doublet potential energy surface diagram corresponds to $\text{C}_5\text{H}_9\text{O}\cdot \rightarrow \text{H} + \text{C}_5\text{H}_8\text{O}$.

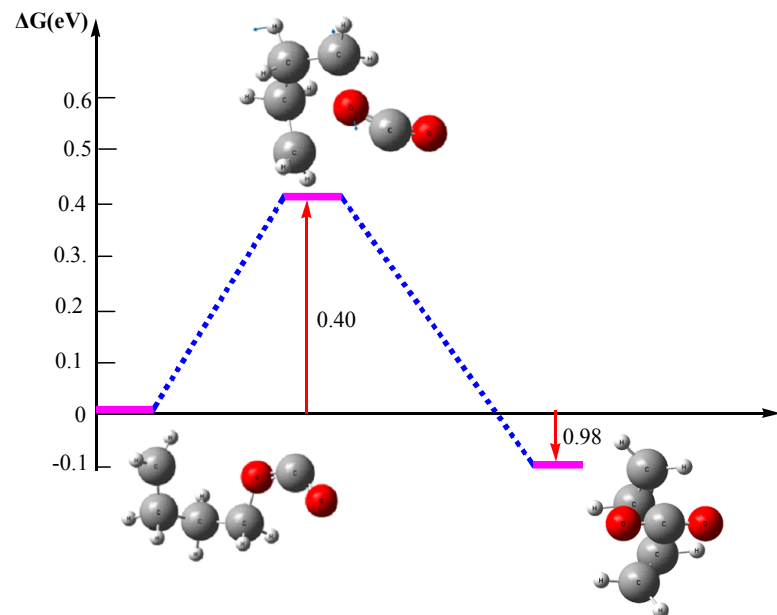


Fig 9. The triplet potential energy surface diagram corresponds to $\text{C}_5\text{H}_8\text{O} + {}^3\text{O} \rightarrow \text{CO}_2 + \cdot\text{C}_4\text{H}_8\cdot$.

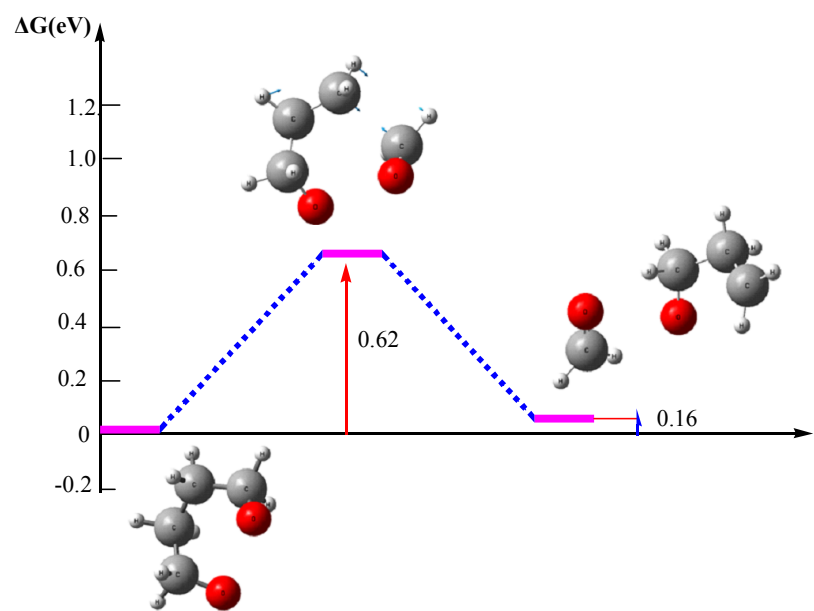


Fig 10.The triplet potential energy surface diagram corresponds to $\cdot\text{OC}_4\text{H}_8\text{O}\cdot \rightarrow \text{C}_3\text{H}_6\text{O} + \text{CH}_2\text{O}$.

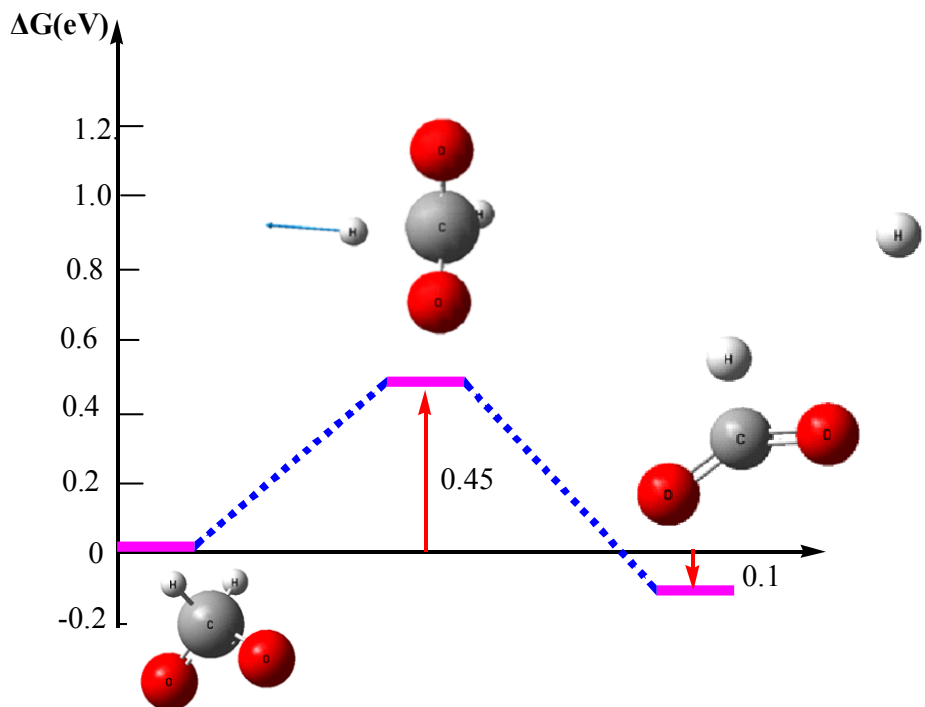


Fig 11.The doublet potential energy surface diagram corresponds to $\text{CH}_2\text{O} + {}^3\text{O} \rightarrow \text{HCO}_2 + \text{H}$.

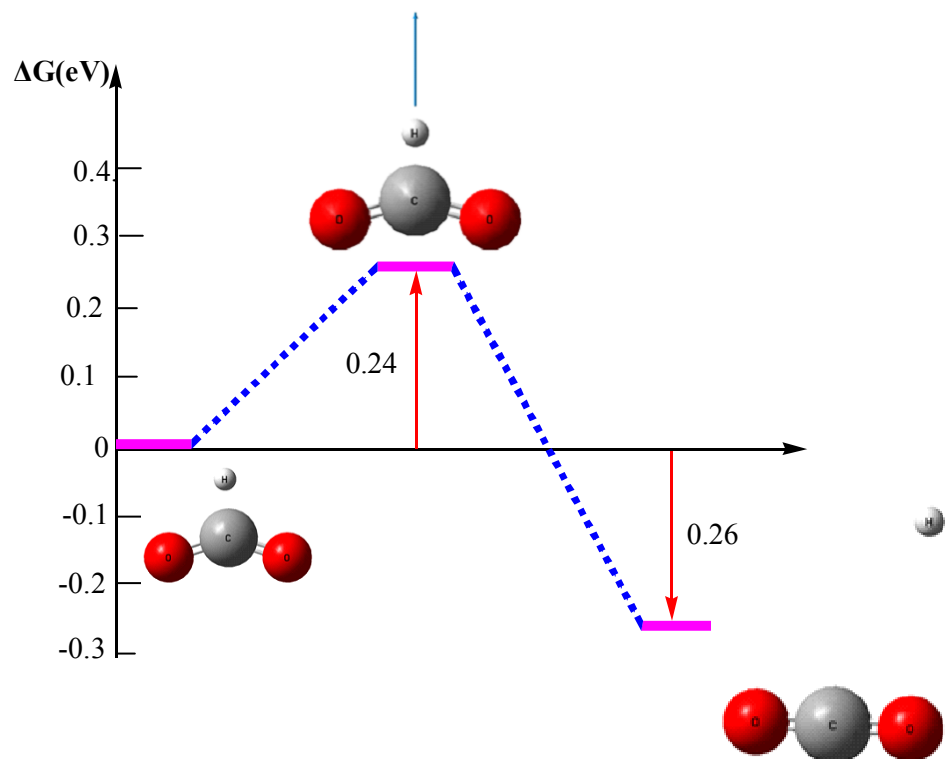


Fig 12.The doublet potential energy surface diagram corresponds to $\text{HCO}_2 + {}^3\text{O} \rightarrow \text{CO}_2 + \text{H}$.

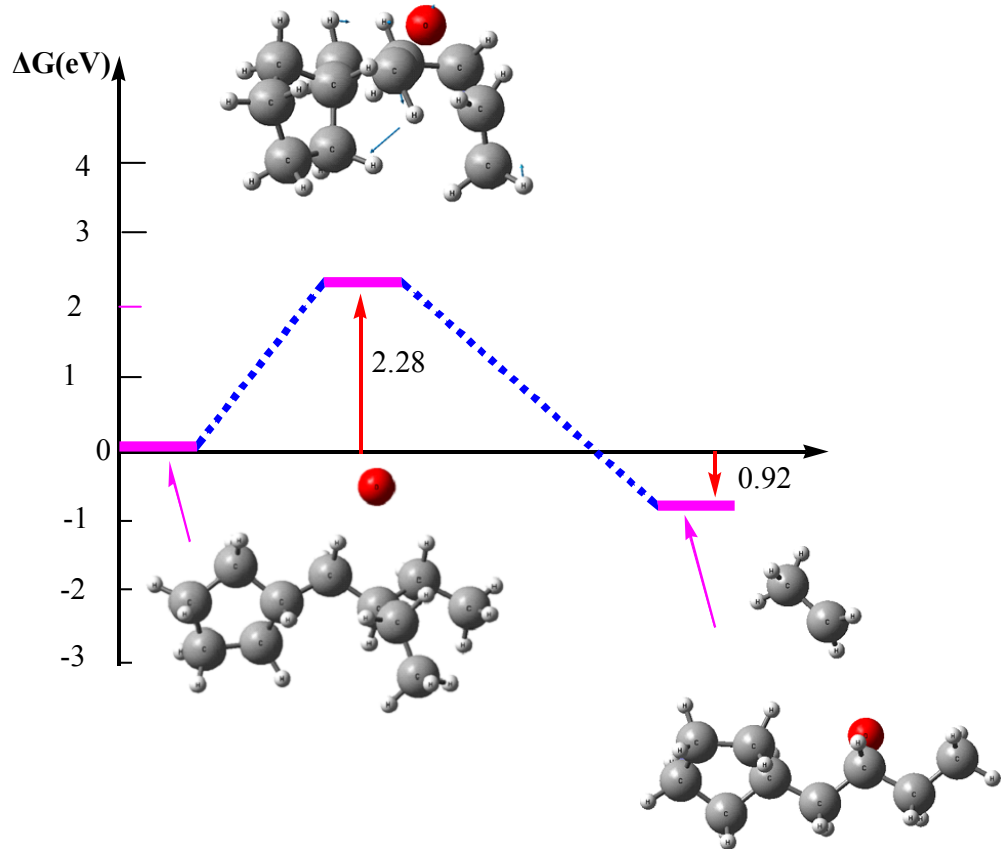


Fig 13.The triplet potential surface diagram corresponds to ${}^3\text{O}$ erosion of L_2 .

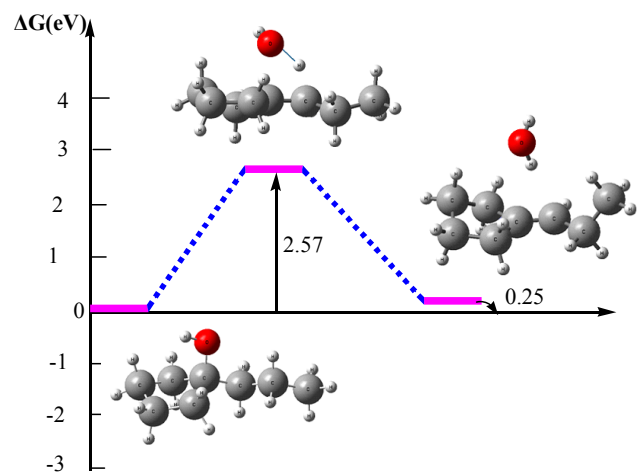


Fig 14.The singlet potential surface diagram corresponds to ${}^1\text{O}$ erosion of L_1 .

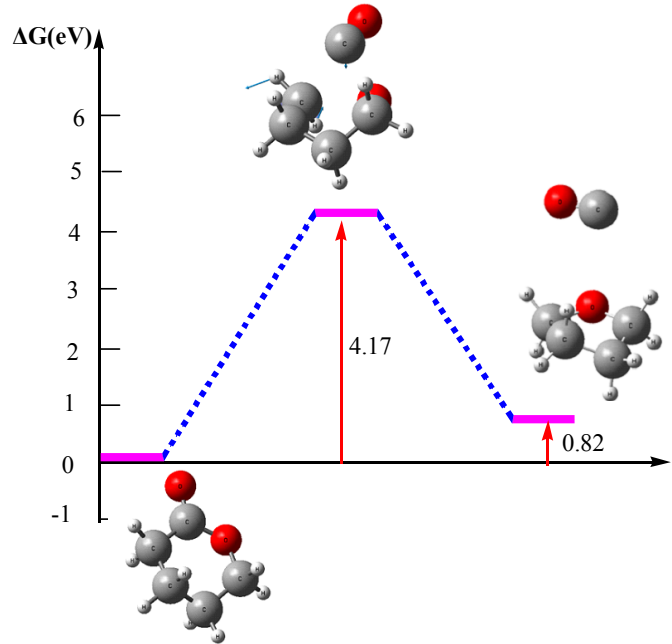


Fig 15.The singlet potential surface diagram corresponds to ${}^1\text{O}$ erosion of cyclopentanone.

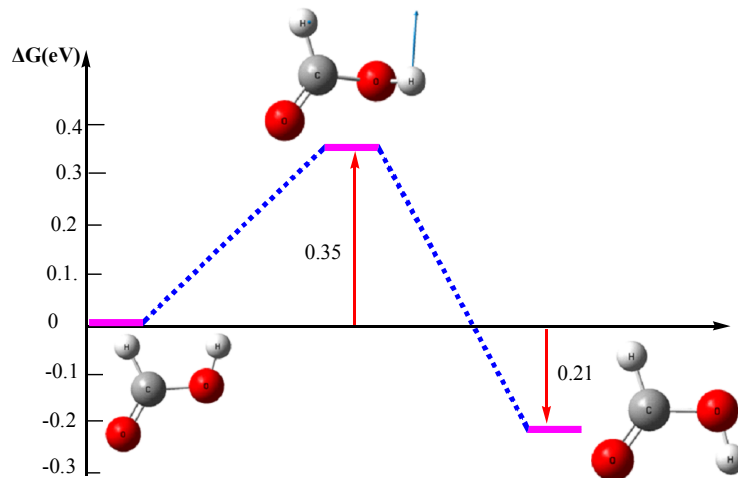


Fig 16.The singlet potential surface diagram corresponds to ${}^1\text{O}$ erosion of formaldehyde.